Ionospheric Rates of Change

Todd Walter and Juan Blanch
Stanford University

Lance de Groot and Laura Norman
NovAtel

Mathieu Joerger
University of Arizona

Abstract
Predicting and bounding the ionospheric rates of change that affect Global Navigation Satellite System (GNSS) signals is of interest for filtering and processing GNSS signals. Although dual frequency measurements may be used to directly estimate and remove the effects of ionospheric variation, there are situations where continuous measurements from more than one frequency may be limited. Further, there may be more advantageous ways to combine information from multiple frequencies, particularly when the ionospheric rates are small. This paper presents an analysis of the potential error of this ionospheric rate estimate under both nominal and disturbed ionospheric conditions using historical data, including previously identified extreme ionospheric events.

Introduction

It is important to understand how the observed ionospheric delay may vary over time. In particular, this paper is concerned with bounding the possible errors that may occur when trying to predict future ionospheric delay values. The primary data used in this study is from the United States and was collected by the Wide Area Augmentation System (WAAS) [1] starting from the year 2000. WAAS collects 1Hz data using receivers that are specifically tuned to maximize data availability under disturbed conditions.

Through our WAAS experience we have seen that the largest known and well-sampled disturbances over the United States occurred between 2000 and 2004 [2]. Since that time, the ionosphere simply has resulted in smaller delays with lower variability. We are currently in a solar minimum period, but it is unknown whether future peaks will be higher or lower than the recent ones. Thus, we need to be prepared for future solar activity that could be comparable to the worst we have seen in the past.

A nominal solar minimum day will have rates on the order of millimeters/sec or below. We have found that 95% of the data from the worst observed days had slant rate values below 8 mm/sec. However, there were occasionally extreme rate values in excess of 150 mm/sec. Fortunately, these latter events are very rare.

Ionospheric Variability

An important consideration is that ionospheric behavior is non-stationary. It changes over the course of the day, over the different seasons, and over an 11-year cycle due to the Sun's changing magnetic field. Further, solar disturbance (e.g. solar flares and coronal mass ejections) can create significant, sudden, and unpredictable variations. We have noticed that changes to the ionospheric behavior are greatest when the background ionosphere is largest (days with 20 m of nominal vertical ionospheric delay will have greater variation than days with 5 m of nominal vertical ionospheric delay). Thus, the greatest variations tend to occur during solar maximum years. Further, the most recent solar maximum (~2011 - 2016) was substantially smaller than previous ones, see Figure 1, which shows the sunspot variation over the last 33 years. Sunspots correlate with the strength of the ionizing radiation that creates the ionosphere. The larger sunspot numbers generally correlate with larger overall ionospheric delay values and therefore larger daily changes in the ionosphere.

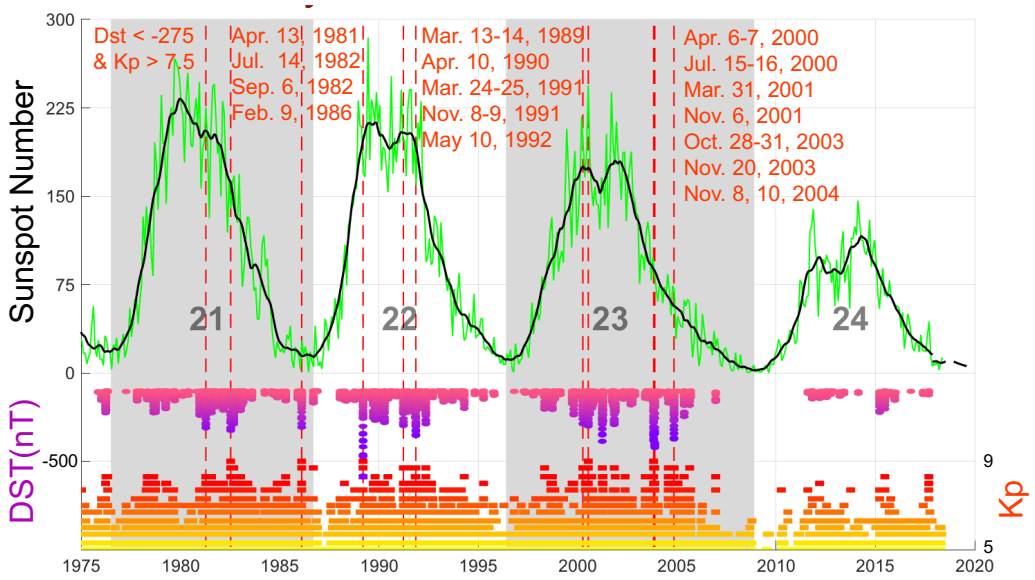

Figure 1. The 11-year solar cycle. This plot shows the monthly sunspot number (green) and its smoothed value (black from 1975 onwards, the dots and squares below identify conditions where the ionosphere had greater disturbance.

The filled ovals in the lower part of Figure 1 show the Disturbance storm time (Dst) index which is a measure of the strength of the Earth's magnetic field [3]. As the Dst becomes more negative, it indicates that solar effects are weakening the magnetic field and the ionosphere is more likely to be disturbed. Values below -50 nano-Tesla (nT) are used to indicate the presence of a geomagnetic storm. Only times when the Dst is below -50 nT are included in the plot. The squares below the Dst values show the planetary K-index (K_p) which is a measure of the variability of Earth's magnetic field. K_p values range from 0 to 9, and values 5 and above are considered to be another indication of geomagnetic storms. Squares are only plotted for times when K_p is 5 or above. We have further used these values to identify extreme storms. In this case, we identify days when Dst is below -275 nT and Kp is greater than or equal to 7.7 as being indicative of extreme storms. Sixteen extreme storms are identified using this method. Extensive analysis of WAAS data (available beginning January 2000) has shown that the ionospheric behavior on the extreme storm days contains substantially larger gradients than on other days. We have processed the WAAS data collected (including the last 7 extreme storm days) to evaluate an upper-bound on ionospheric rate errors.

Unfortunately, data collected prior to the year 2000 was generally collected at too low of a sample rate (usually every 30 seconds or longer) and is of lower quality (earlier L2 tracking methods often could not keep up with rapid ionospheric variations and would lose data during disturbed periods). WAAS collects 1Hz data using receivers that were specifically tuned to maximize data availability under disturbed conditions. We have also examined ionospheric rates from other parts of the world. It is well known that equatorial regions have larger ionospheric delays including high variability in the post sunset hours when the suns radiation stops ionizing the atmosphere and the free electrons recombine with the positive ions. Unfortunately, reliable high rate data GNSS from these regions prior to 2005 is difficult to obtain. We have processed RINEX data from South America known to contain very large spatial gradients (March 1, 2014) as compared to North American data.

The primary data for this study comes from WAAS for the following extreme storm days:

- April 6-7, 2000
- July 15-16, 2000
- October 29-30, 2003
- November 20, 2003

These days contain the largest well-observed ionospheric disturbances in the WAAS data set. The data sets are so-called supertruth data. Supertruth is a WAAS term for data that has been collected and processed from each of three co-located reference receivers. Continuous arcs of carrier phase estimates of the ionosphere are identified, one line of sight (LOS) between a satellite and a reference station at a time, and then each LOS has its ambiguity bias estimated and removed. The

resulting LOS tracks for the three co-located reference receivers are compared to one another using voting to identify and eliminate outliers caused by tracking problems or other non-ionospheric behavior. The median LOS track of the three is selected as the best measurement for that location to that satellite (provided all three are within a few cm of each other). The result is a very clean and low-noise estimate of the ionosphere.

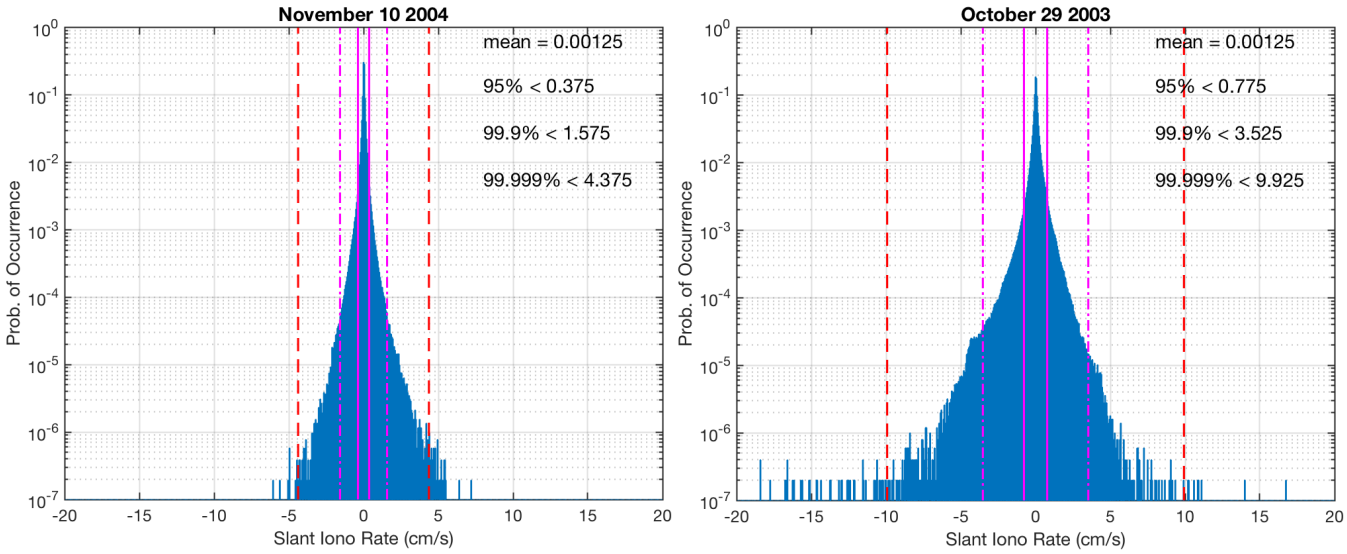

Figure 2. Histograms of slant ionospheric delay rates for (a) November 10, 2004 and (b) October 29, 2003.

Figure 2 shows the distribution of ionospheric slant rates for two different days. A minorly disturbed day: November 10, 2004, and the day with the largest gradients: October 29,2003. The figure also shows the mean values as well as the 95%, 99.9% and 99.999% containment bounds. Notice the difference between the two distributions, particularly in the tails. The left side showing November 10, 2004 is a moderately disturbed day whose largest rate is below 60 mm/s. The right-side showing October 29, 2003 has the largest observed gradients of just over 174 mm/s. Notice that the containment bounds are all approximately twice as large. These represent values that are somewhat larger than typical and much larger than typical.

We also obtained Brazilian data that has been processed by KAIST that corresponds to March 1, 2014. KAIST has identified this set as containing large spatial ionospheric gradients [4]. This data is collected at a lower rate (every 15 seconds) and does not contain co-located receivers. Thus, the process of removing receiver errors and other spurious artifacts is less accurate. We have found it to contain fewer continuous arcs which means the data is more limited for examining changes in the ionosphere over time. The observed rates of change from this Brazil data were well below the maximum values from the WAAS data set.

Prediction Error Processing

We began by investigating the magnitude of the slant ionosphere delay change over different time intervals. For each data point that belonged to a continuous arc of data between a receiver and a satellite, we computed the change in ionospheric slant delay versus the change in time. These values were recorded into a set of histograms at each time step from five seconds to two-hundred seconds after the initial point. Values were recorded for all measurements that had subsequent points belonging to the same continuous arc. In this analysis, the ionosphere is treated as though it will remain unchanged from the initial value. The corresponding prediction error is the difference between the later slant delay value and the initial value.

The data was next used to estimate the ionospheric rate of change for each line of sight observed during these extreme storms. Of interest to us was its departure from linear behavior. Large gradients do not pose a significant challenge to differential systems if they are slowly changing and predictable. In this paper we are looking at not just the gradient values, but how accurately they may be predicted over time. Differential corrections will have both latency as well as limited update rates. Further, corrections may not reach the user and they may need to forward predict an old estimate for an

extended time. This process is intended to evaluate the accuracy of a simple linear prediction of the ionosphere given past data.

For a specific continuous arc of data, two minutes of measurements (24 samples of 5-second supertruth data) were fit to a straight line and used to obtain the ionospheric rate estimate. This rate was then applied to the last measurement of the fit and used to predict the next 200 seconds of data. Our intent is to be able to predict for at least two minutes and perhaps longer. The difference between the predicted and actual measurement was tabulated for further analysis. The process was repeated for each line of sight and each possible time-window. That is, we started with the first 24 samples to predict the next 40. Then we would advance 5 seconds and use samples 2-25 to predict values for samples 26-65. This process was repeated for the full continuous arc. Then, the next continuous arc of data was evaluated and the whole process repeated until all of the arcs in each data set were evaluated. We evaluated different fit interval lengths and settled on 120 seconds as it was comparable to the interval over which we wished to predict ionospheric behavior. We obtained similar results when we evaluated different values for this parameter.

Figure 3a shows the worst performing track in the data set. It corresponds to a reference station in Washington DC on October 29, 2003 which was one of the very worst ever solar storms well observed by GPS data. The steepest temporal gradient in the WAAS data set can be seen at about 70 minutes into the arc. Figure 3b illustrates the process. Data is used to form a fit. In this illustrative example only the six circled data points were used (30 seconds) to calculate the ionospheric rate of change. The black line shows the resulting predicted values (with hash marks at the five second intervals) and the dots show the actual measurements. Here the curvature in the ionosphere rapidly builds to many meters of error.

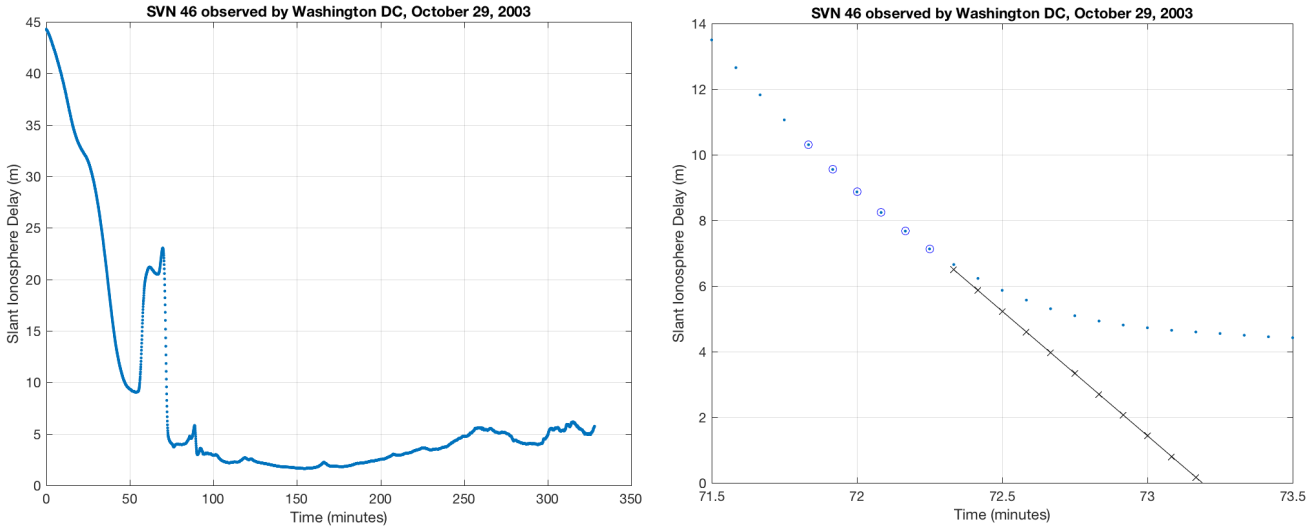

Figure 3. the track with worst performance in the data set (a) and an illustration of the overall process used to evaluate the error (b).

Prediction Error

Histograms of the resulting prediction error (combined over the four previously identified storms) are shown in the subsequent figures. Each five-second predicted interval has a set of colored bars showing the number of times a specific slant delay prediction error value was encountered. Plotted over the top of the histogram data are colored lines showing the percentage of data points that had a prediction error of that value (or lower). The blue lines are the closest to zero on these plots and represent 95% of the data. The black lines show greater growth and represent 99.9% of the data. The red lines bound 99.999% of the data. Tables are also provided with specific numerical values.

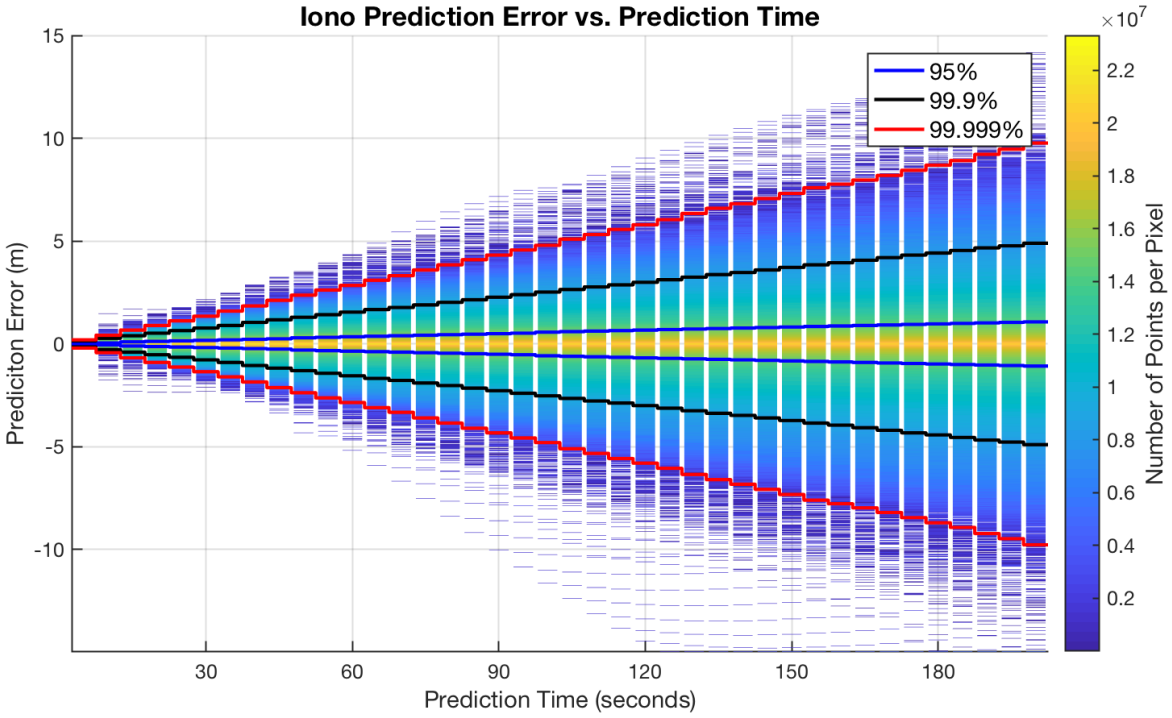

Figure 4. Histogram of slant iono change over time.

Time (sec)	99.9% Error (m)	99.999% Error (m)	Maximum Error (m)
10	0.275	0.43	1.75
20	0.525	0.9	2.36
30	0.775	1.35	2.29
40	1.05	1.85	2.88
50	1.3	2.38	4.34
60	1.55	2.85	5.17
70	1.775	3.33	6.67
80	2.025	3.85	8.37
90	2.275	4.33	10.03
100	2.525	4.8	11.63
110	2.775	5.33	13.13
120	3	5.8	14.45
130	3.25	6.35	15.56
140	3.475	6.83	16.46
150	3.725	7.33	17.12
160	3.95	7.78	17.59
170	4.2	8.2	17.88
180	4.425	8.7	18.11
190	4.675	9.22	18.27
200	4.9	9.78	18.39

Table 1. Slant ionospheric change versus time

Figure 4 and Table 1 present the results when the ionosphere is held constant over the time periods of evaluation. The 99.999% bound has a slope of approximately 49 mm/sec. The outliers initially grow at a rate of 175 mm/sec for the first 20 seconds and then at a rate of about 90 mm/sec thereafter. Thus, the maximum instantaneous rate of ~175 mm/sec is not sustained for more than about 20 seconds in our dataset. Figure 5 and Table 2 show the results when a slope is estimated and used to predict the future ionospheric values.

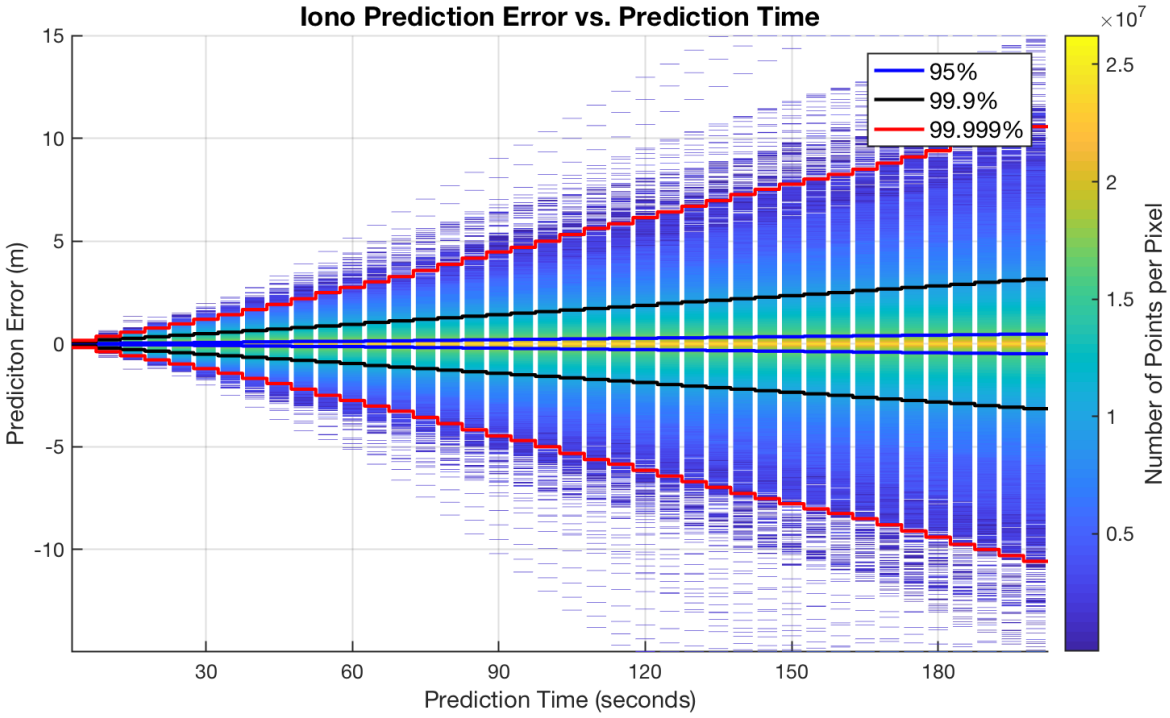

Figure 5. Histogram of linear prediction error.

Time (sec)	99.9% Error (m)	99.999% Error (m)	Maximum Error (m)
10	0.20	0.38	0.65
20	0.35	0.78	1.31
30	0.50	1.20	1.99
40	0.65	1.68	3.08
50	0.80	2.20	4.21
60	0.95	2.75	5.14
70	1.10	3.28	6.63
80	1.275	3.88	8.31
90	1.425	4.45	10.19
100	1.575	5.03	12.03
110	1.725	5.62	13.8
120	1.875	6.15	15.48
130	2.05	6.70	16.97
140	2.20	7.25	18.26
150	2.35	7.78	19.33
160	2.50	8.28	20.17
170	2.675	8.80	20.90
180	2.825	9.40	21.52
190	2.975	10.00	22.35
200	3.15	10.58	23.68

Table 2. Linear ionospheric prediction errors versus time

Nominally, even on these extreme storm days, the iono rate prediction is very accurate for the next 200 seconds. However, from the data, we can see that some extreme ionospheric events can cause errors that are more than an order of magnitude worse than typical. Even short prediction times (ten seconds) can have errors corresponding to more than half a meter in extreme cases. Further, the error distribution is non-Gaussian as it has very fat tails. Such days are rare in mid-latitudes, only occurring less than once or twice a year on average (more often near solar max and less frequently during solar min). We can go entire years without seeing such behaviors. Indeed, we have not seen quite as extreme behavior

since 2003. However, there were many disturbance events after 2003 that would have produced errors far greater than what would be expected on a typical day. Unfortunately, ionospheric disturbances can strike quite suddenly, and it can be very difficult to predict that such an event is about to occur from the data used to perform the fit.

Surprisingly the 99.999% bound at 53 mm/sec is slightly worse than the prior case when not extrapolating the slope. The linear model appears to be better in the short term. The outliers are bounded by 66 mm/sec for the first 30 seconds and then by 128 mm/sec thereafter. Linear prediction leads to smaller error bounds for the first 30 seconds, but they are then comparable out to ~110 seconds and worse thereafter. The linear prediction leads to better accuracy as the 95% and 99.9% bounds are much reduced.

The next sections evaluate two possible mitigations for reducing these required error bounding values. The first method identifies the second largest gradient value observed at each reference station during such disturbances. This approach could be used in combination with Receiver Autonomous Integrity Monitoring (RAIM) [5]. This approach relies on an assumption that the worst error could be identified by RAIM and that two such extreme prediction errors would be sufficiently unlikely to affect two different lines of sight for the same user at the same time. The second method uses metrics for evaluating the goodness of fit and large ionospheric rates to identify and exclude extreme conditions.

Bounding Combined with RAIM

If we assume that RAIM will identify the worst-case single satellite prediction error cases and that the threat events described above are very rare, then perhaps it is not necessary to bound the worst possible case. RAIM could identify this worst case (provided the probability of exceeding the expected case is small compared to the assumed likelihood of individual fault) and instead we only need to bound the next largest prediction error. We therefore re-processed the data to discard the largest observed error at any given reference receiver at each given time step. Figure 6 shows the resulting histogram. Note that the overall error growth is only about a third of the previous case, with a 99.999% growth rate of about 24 mm/sec. The maximum error can be bounded by an upper limit of 36 mm/sec.

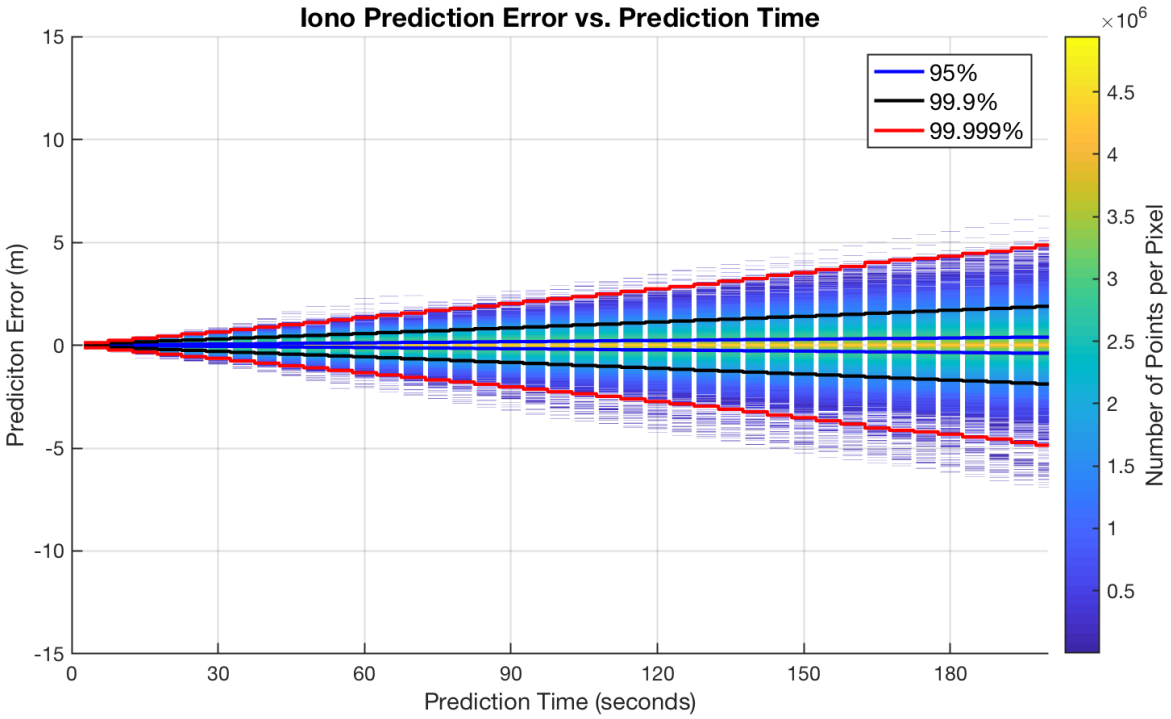

Figure 6. Histogram of iono rate prediction error (excluding the largest predicted error at any station at each time).

Time (sec)	99.9% Error (m)	99.999% Error (m)	Maximum Error (m)
10	0.113	0.24	0.36
20	0.213	0.44	0.68
30	0.3	0.64	0.93
40	0.388	0.88	1.3
50	0.475	1.1	1.88
60	0.562	1.34	2.26
70	0.663	1.56	2.42
80	0.75	1.79	2.83
90	0.838	2.02	3.16
100	0.938	2.26	3.57
110	1.025	2.49	3.81
120	1.125	2.74	4.23
130	1.225	2.96	4.52
140	1.312	3.24	4.82
150	1.4	3.53	5.24
160	1.5	3.83	5.58
170	1.6	4.14	5.86
180	1.7	4.33	6.17
190	1.788	4.56	6.6
200	1.888	4.86	6.91

Table 3. Ionospheric prediction errors versus time (excluding the largest error at any station at any time)

More study is needed in order to determine if this method is valid. One limitation is that the data used here only contained GPS satellites. However, had more satellites from different constellations been available, it is possible that the second largest error would be larger than what is seen in this data set. The more satellites in the sky, the more likely two satellites are to be close together and perhaps to both sampling the ionospheric behavior from the worst portion of the sky. We believe this idea still has merit, but it should be evaluated further before taking full credit for the findings presented here. Concepts from Advanced RAIM (ARAIM) [5] could potentially be utilized to test for simultaneous faults on groups of satellites that are sufficiently close together.

Screening Based on Fit Results

The next approach is to not use the prediction when the calculated rates of change become too large. Large rate values can be indicative of disturbed days and of when the predicted error is likely to be worse. We limited the slope values to 3 mm/second as such values are not typically observed on nominal days. We also included a chi-square check on the data as there were times during disturbed intervals when the ionospheric rate changed sign and briefly met this criterion, but then resulted in large prediction errors. This occurred because the slope passes through zero when it changes sign. The chi-square checks are able to detect when obvious curvature is present and prevent such cases from leading to less accurate predictions.

The chi-square metric is the sum of the fit residuals (the 120 actual measurements minus their fit predicted values) divided by the estimated measurement sigma value and then squared before summing. We used a sigma values that had been estimated for the supertruth accuracy that ranged from about 1 cm to ~35 cm, with most being around 3 cm. The chi-square threshold was set to an empirical value of 1.5 times the number of points used in the fit. For 5 second data we used 24 points and set the threshold at 36. This threshold requires tuning depending on how conservative the sigma estimates of any data set are compared to the actual measurement noise. The supertruth sigma estimates are considered to be rough values and do not necessarily have high degree of accuracy.

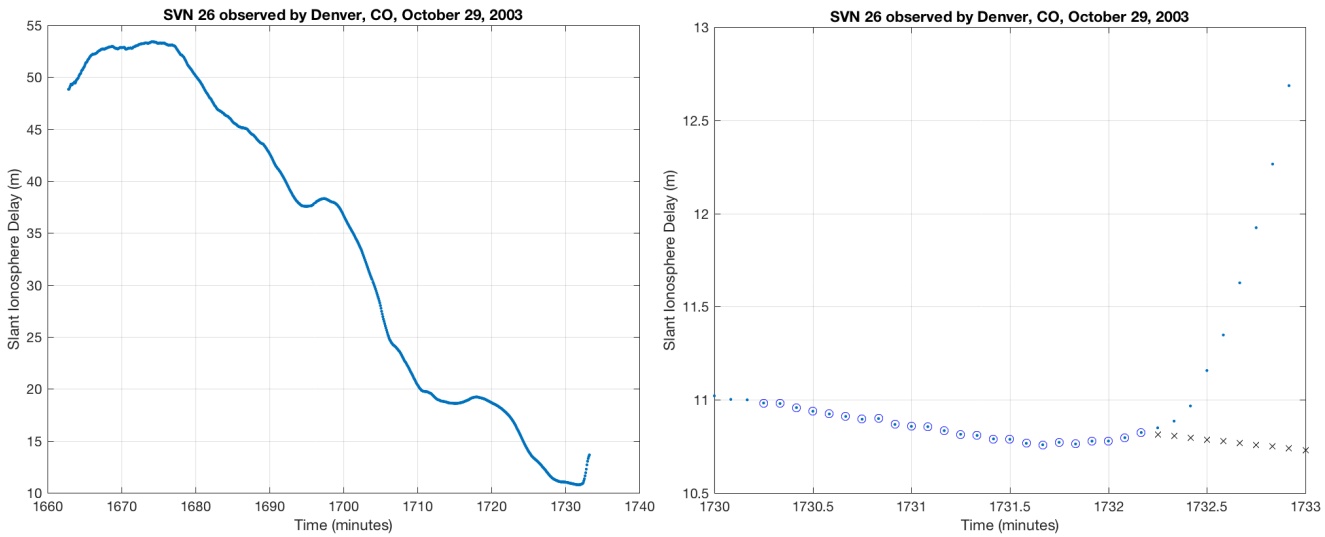

Figure 7. A track with a small slope, but still somewhat poor prediction (a) and an illustrative example of the data used to evaluate the error (b).

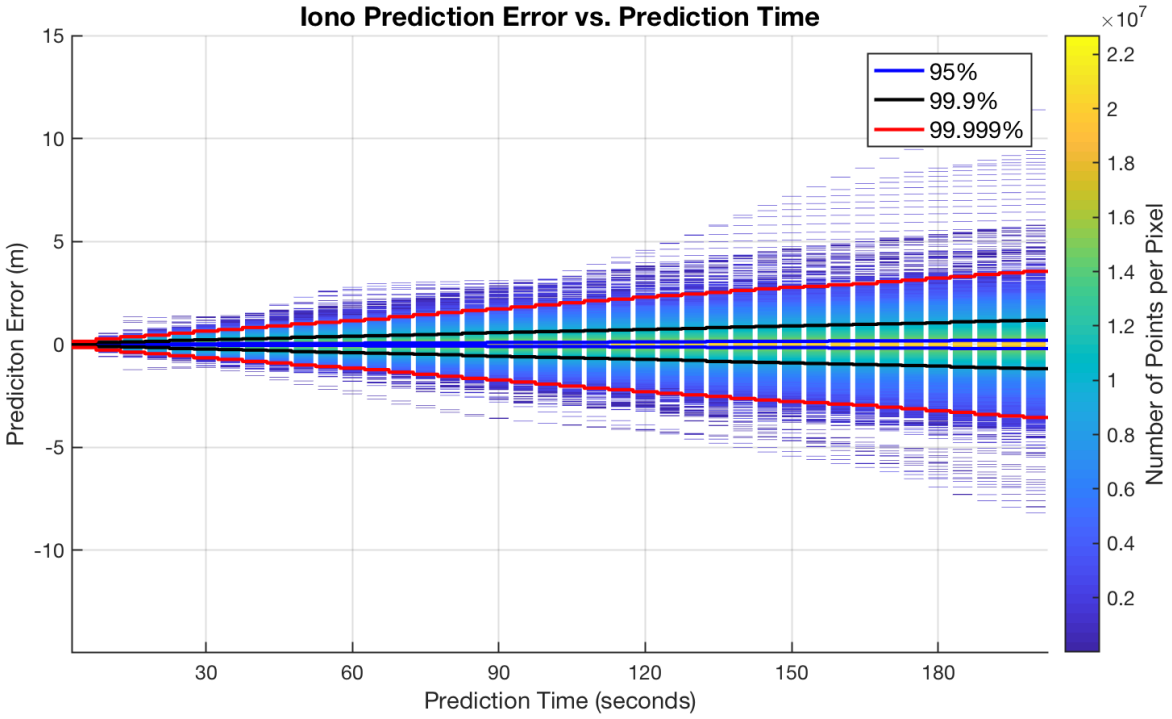

Figure 8. Histogram of iono rate prediction error (excluding cases with a slope above 3 mm/sec or large chi-square values).

Figure 7 shows one of the worst resulting tracks. The 24 circled points were used to estimate the slope and obtained a relatively small rate estimate with a sufficiently low chi-square value. However, shortly after the estimation process, the ionospheric rate significantly increased. Despite such occurrences we found that the slope checks did eliminate many bad tracks and resulted in a noticeable prediction accuracy improvement. Figure 8 shows the new histogram and Table 4 has the specific values. Here the 99.999% growth rate is about 22 mm/sec. The maximum error is bounded by an upper limit of 61 mm/sec.

This slope check roughly cuts the magnitude of the error growth in half compared to Figure 5. We have not further evaluated tighter slope or chi-square thresholds, but further optimizations are certainly possible. This implementation was performed on a satellite-by-satellite basis and did not retain any memory of past trips. We could also examine an algorithm that prevents prediction once any satellite sees a large slope and perhaps continue to deny prediction until all slopes are below a limit for an extended time. Such an algorithm could be much better at identifying disturbed days. However, it also risks denying availability should there be a false alert due to non-ionospheric induced tripping, such as multi-path.

Time (sec)	99.9% Error (m)	99.999% Error (m)	Maximum Error (m)
10	0.10	0.28	0.61
20	0.15	0.45	1.31
30	0.225	0.65	1.36
40	0.275	0.83	1.53
50	0.35	1.00	2.31
60	0.40	1.15	2.77
70	0.45	1.35	2.99
80	0.50	1.55	3.30
90	0.575	1.73	3.61
100	0.625	1.93	3.84
110	0.675	2.12	4.02
120	0.725	2.30	4.59
130	0.775	2.45	5.33
140	0.85	2.62	6.27
150	0.90	2.78	7.20
160	0.95	2.90	8.12
170	1.00	3.05	9.05
180	1.05	3.23	9.89
190	1.125	3.40	10.68
200	1.175	3.55	11.39

Table 4. Ionspheric prediction errors versus time (excluding cases with a slope above 3 mm/sec or large chi-square values)

Combined RAIM and Fit Based Screening

The last evaluation method looks into applying both improvements together: removing the largest error at any given reference location and limiting usage based on the predicted ionospheric rates. The results of this last algorithm are shown in Figure 9 and Table 5. As expected, this approach leads to the smallest resulting error: roughly six times smaller than the values in Figure 5 and Table 2. This is in line with the product of the factors obtained from the individual improvements from the previous sections. The combined 99.999% growth rate is about 10 mm/sec. The maximum error can be bounded by an upper limit of 23 mm/sec for the first 20 seconds and 13.5 mm/sec thereafter.

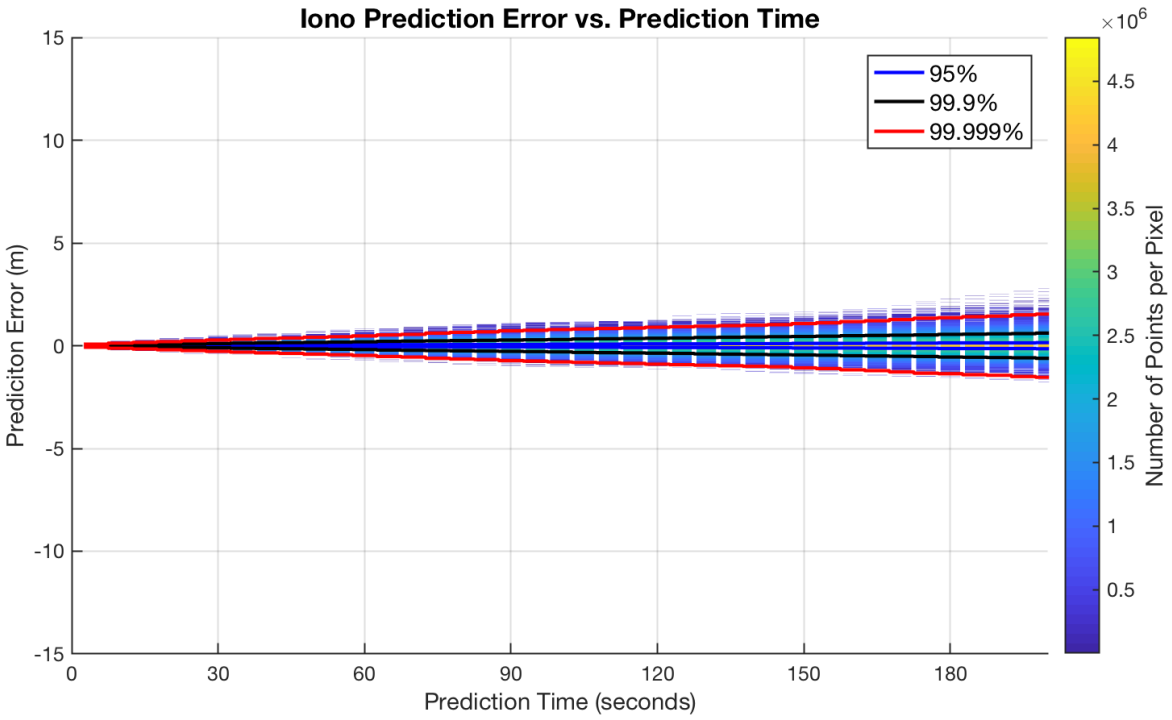

Figure 9. Histogram of iono rate prediction error (excluding the largest error at any station and cases with a slope above 3 mm/sec or large chi-square values).

Time (sec)	99.9% Error (m)	99.999% Error (m)	Maximum Error (m)
10	0.05	0.12	0.23
20	0.075	0.20	0.35
30	0.10	0.28	0.48
40	0.138	0.35	0.58
50	0.163	0.41	0.71
60	0.188	0.48	0.84
70	0.225	0.55	0.90
80	0.25	0.65	1.01
90	0.275	0.73	1.09
100	0.30	0.79	1.14
110	0.338	0.84	1.18
120	0.363	0.90	1.25
130	0.40	0.95	1.53
140	0.425	1.00	1.56
150	0.45	1.07	1.63
160	0.488	1.18	1.74
170	0.513	1.28	1.98
180	0.55	1.36	2.29
190	0.575	1.44	2.52
200	0.613	1.54	2.77

Table 5. Ionospheric prediction errors versus time (excluding the largest error at any station and cases with a slope above 3 mm/sec or large chi-square values)

Equatorial Data

We obtained processed RINEX data from South America courtesy of Professor Jiyun Lee of KAIST. The data set with the largest spatial gradients that her group has observed comes from March 1, 2014 [4]. From Figure 1 we can see that this corresponds to the peak of the most recent solar maximum. However, that peak is still considerably smaller than prior solar maximums. These data sets had a 15 second sampling interval. They also contain a higher incidence of cycle slips than were seen in the WAAS data sets. As a result, the observed arc lengths are often shorter. These effects somewhat limit the sampling of the ionospheric behavior. Nevertheless, much of the data was of good quality and we were able to evaluate the continuous arcs that were present in the data. Although Professor Lee observed larger spatial gradients in this data set than any found in the WAAS data set, we found that the predicted ionospheric errors were much smaller than we obtained from the WAAS data. This requires further investigation to confirm that it is a correct representation of the data and that the larger errors are not unintentionally screened by the missing data. Figure 10 shows the histograms for this data set and Table 6 has specific values.

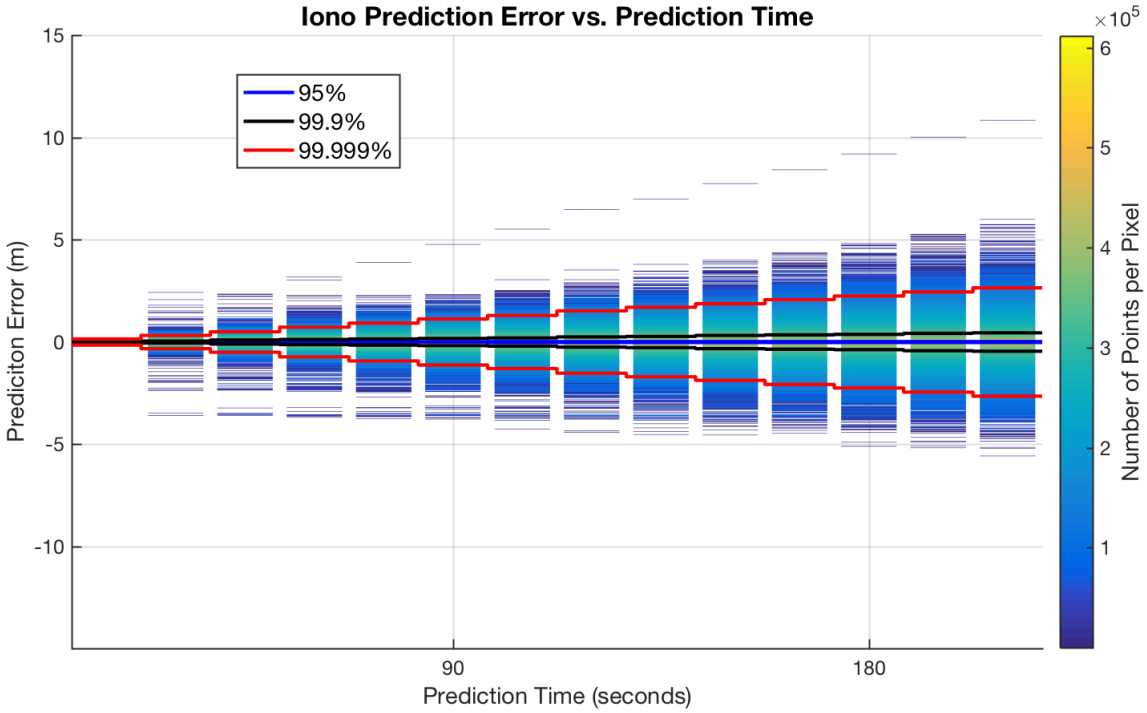

Figure 10. Histogram of iono rate prediction error in South America.

The values do indicate some large changes in the ionospheric rate were present, but not nearly as large as what was seen for mid-latitude storm days. The 99.999% growth rate is only about 12.5 mm/sec. The maximum error can be bounded by an upper limit of 120 mm/sec for the first 30 seconds and 40 mm/sec thereafter. Even in the storm day WAAS data we did not see perfect correspondence with large spatial gradient and large temporal gradients. However, we are somewhat surprised to obtain such low values given the size of the reported spatial gradients in this data set. Maximum spatial gradients and maximum temporal gradients do not always align. Although they are expected to often occur together, the maximum value of one does not necessarily imply a maximum value for another. It certainly seems likely that larger values in Brazil may be found with an examination of a larger data set.

Time (sec)	99.9% Error (m)	99.999% Error (m)	Maximum Error (m)
30	0.05	0.325	3.59
60	0.125	0.725	3.67
90	0.175	1.125	4.77
120	0.25	1.525	6.47
150	0.325	1.875	7.74
180	0.375	2.25	9.20
210	0.45	2.65	10.85

Table 6. Ionospheric prediction errors versus time for South America

Conclusions

The maximum observed rate of change of the slant ionosphere is 175 mm/sec. This observation occurred during one of the most extreme ionospheric disturbance events to have been monitored with dense sampling of good quality GNSS measurements. Previous solar cycles have had larger disturbances but were not adequately sampled and the subsequent solar cycle has had no such disturbances. It is therefore possible that worse gradients may be observed in the future. However, such events should be exceedingly rare. We showed that by estimating the ionospheric rate of change and applying it to predict ionospheric delays for the next few minutes generally improved accuracy compared to simply using the last measured value. However, we also showed that the maximum error resulting from this linear extrapolation was only improved for the first 20 seconds and that thereafter these errors were comparable and then even worse after about two minutes.

By applying the rate limit and excluding the worst value observed at any location, we obtained an upper bound on the prediction error of about 23 mm/sec. If we assume that this corresponds to roughly a 5-sigma error, then one can assume a one-sigma error bound on the order of 5.2 mm/sec for the worst observed ionospheric prediction rate. Thus, after 30 seconds forward prediction time, the 1-sigma error bound can be set to 16 cm. This value should bound all but the very worst gradients that pass the 3 mm/sec estimation rate limit. The values that it does not bound are likely to be sufficiently rare to be detected by the RAIM algorithm. There may be other ways to further lower this upper error bound by combining information across different satellites in order to more effectively identify days that have unusual ionospheric activity.

References

[1] Lawrence, Deborah, Bunce, Deane, Mathur, Navin G., Sigler, C. Edward, “Wide Area Augmentation System (WAAS) - Program Status,” Proceedings of the 20th International Technical Meeting of the Satellite Division of The Institute of Navigation (ION GNSS 2007), Fort Worth, TX, September 2007, pp. 892-899.

[2] Datta-Barua, Seebany, “Ionospheric Threats to Space-Based Augmentation System Development,” Proceedings of the Institute of Navigation's GNSS Meeting, Long Beach, California, September 2004.

[3] Datta-Barua, Seebany, Walter, Todd, Blanch, Juan A., and Enge, Per K, “Can WAAS Availability Be Inferred From Geomagnetic Data? An Analysis,” Proceedings of the Ionospheric Effects Symposium 2005, Alexandria, Virginia: 3-5 May 2005.

[4] M Yoon, D Kim, J Lee, “Validation of Ionospheric Spatial Decorrelation Observed During Equatorial Plasma Bubble Events,” IEEE Transactions on Geoscience and Remote Sensing 55 (1), 261-271, 2017.

[5] Blanch, Juan A., Walter, Todd, Enge, Per K., Lee, Y., Pervan, Boris S., Rippl, M., Spletter, A., Kropp, V, “Baseline Advanced RAIM User Algorithm and Possible Improvements,” Published in IEEE Transactions on Aerospace and Electronic Systems, Volume 51, No. 1, January 2015.